The Impact of Neuronal Structure on Cortical Network Architecture

Daniel Udvary[1], Philipp Harth[2], Jakob H. Macke[3], Hans-Christian Hege[2], Christiaan P.J. de Kock[4], Bert Sakmann[5], Marcel Oberlaender[1,*]

[1]Max Planck Group: In Silico Brain Sciences, Center of Advanced European Studies and Research (caesar), Ludwig Erhard Allee 2, 53175 Bonn, Germany. [2]Department of Visual and Data-centric Computing, Zuse Institute Berlin, Takustraße 7, 14195 Berlin, Germany. [3]Machine Learning in Science, Tübingen University, Maria von Linden Straße 6, 72076 Tübingen, Germany. [4]Department of Integrative Neurophysiology, Center for Neurogenomics and Cognitive Research, VU Amsterdam, De Boelelaan 1085, 1081 Amsterdam, the Netherlands. [5]Max Planck Institute of Neurobiology, Am Klopferspitz 18, 82152 Martinsried, Germany.

*** Editorial correspondence:** Max Planck Group: In Silico Brain Sciences, Center of Advanced European Studies and Research (caesar), Ludwig-Erhard-Allee 2, Bonn, 53175 Germany, marcel.oberlaender@caesar.de

It has become increasingly clear that the neurons in the cerebral cortex are not randomly interconnected. This wiring specificity can result from synapse formation strategies that interconnect neurons depending on their activity or genetically defined identity. Here we found that in addition to such synapse formation strategies, the structural composition of the neuropil provides a third prominent source by which wiring specificity can emerge in cortical networks. This structurally determined wiring specificity reflects the packing density, diversity and similarity of the neurons' dendritic and axonal processes. The higher these three factors, the more recurrent the networks' topology. Conversely, lower density, diversity and similarity yield feedforward networks. These basic principles predict connectivity patterns from subcellular to network scales that are remarkably consistent with empirical observations from a rich body of literature. Thus, cortical network architectures reflect the specific morphological properties of their constituents to a much larger degree than previously thought.

Introduction

Neuronal networks are implemented in the brain via a plethora of molecular mechanisms, which form synaptic connections between the neurons' long and branched dendrites and axons (*1-5*). Axo-dendritic proximity is hence necessary for the formation of synapses and constrains which neurons could in principle be connected to one another – and where along their neuronal processes these connections could occur. Yet it is unclear, whether and to what degree the highly diverse morphological properties of neurons can impact the architecture of the networks they form (*6*). For the past decades, the common strategy for investigating the impact of neuronal structure on network architecture has been to test the validity of 'Peters' Rule' (*7*). According to this longstanding hypothesis, axons form synaptic connections randomly wherever they get in close proximity to a dendrite (*8*). Proximity would hence not only be necessary, but sufficient to account for connectivity. Consequently, Peters' Rule can be simply restated as "proximity predicts connectivity". If this were true, the morphological properties of neurons would directly determine the architecture of neuronal networks, independent of the particular molecular mechanisms that form synapses.

Tests of Peters' Rule have consistently failed to support it (*9-13*). At subcellular scales, dense reconstructions showed that dendritic spines, for example in mouse somatosensory cortex, are in close apposition to ten axonal branches, of which on average only one establishes a synapse (*12*). Moreover, a subset of these axonal branches formed synaptic clusters by connecting to several close-by spines along the same dendrite (see also (*13*)). At cellular scales, sparse reconstructions showed that axo-dendritic proximity is insufficient to account for the patterns of synaptic connections (*14*), or for differences in connection probabilities that reflect the neurons' cell types (*11*). Because they falsify Peters' Rule directly, such observations are considered to reflect wiring principles that are independent of neuronal structure. Thus, the absence of synaptic connections between close-by dendrites and axons, and the occurrence of synaptic clusters between them, are commonly interpreted as the result of synapse formation strategies that interconnected these neurons based on their cellular identity, cell type or activity (*12*).

Interpreted as further evidence for this conclusion are observations which showed that neurons form particular network motifs – for example feedforward loops – that occur more (or less) frequently than expected for randomly connected networks (*15, 16*). Theoretically, such nonrandom topological properties could very well arise from simple sets of wiring rules (*4, 5*) or via learning (*17*), and therefore be independent of the morphological properties of neurons. However, even if neurons were interconnected randomly by axo-dendritic proximity, the resulting networks would also display complex connectivity patterns (*18, 19*) and generally nonrandom topologies (*19, 20*). Furthermore, recent work showed that morphological properties – such as dendrite polarity – can represent a defining source for nonrandom occurrences of network motifs (*21*). These observations indicate that falsifying Peters' Rule may be insufficient to unambiguously conclude whether empirically observed wiring specificity reflects morphological properties of the neurons, a particular synapse formation strategy, or combinations thereof. Thus, conclusive answers to the questions – Which principles link neuronal structure to network architecture, and how can these principles be disentangled from those of synapse formation strategies? – remain presently unknown.

Here, we quantitatively address these questions by introducing a statistical modelling approach that can derive how neuronal networks would appear if synapse formation strategies that introduce wiring specificity were absent. We apply this approach to a dense model of the vibrissal related part of the rat primary somatosensory cortex (i.e., barrel cortex; a link to the model and the underlying anatomical data is provided in the **Materials and Methods**). We demonstrate that the model provides realistic and robust estimates for the numbers of axonal and dendritic branches within any subvolume of this brain area, for the synaptic structures that they represent, and for the diversity of their respective cellular and cell type origins. The model revealed that axo-dendritic proximity can in general not predict connectivity, because the number of overlapping branch pairs exceeds the number of synaptic structures by two orders of magnitude. However, beyond Peters' Rule, we found three factors of the neuronal structure that translate into nonrandom pairwise and higher-order connectivity patterns. Because of the mismatch between synaptic structures and branch pairs, the packing density and morphological diversity of neuronal processes affect how sparsely and heterogeneously a network is interconnected. Similarities in projection patterns lead to correlated connectivity. The combination of these three structurally determined factors defines a network's specific nonrandom topology. Tissue with high packing density and cellular diversity thereby yields recurrent network architectures. Low density and diversity yield feedforward architectures. These basic principles predict cell type-specific connectivity patterns, as well as occurrences of synaptic clusters and network motifs that are in remarkable agreement with the available empirical data.

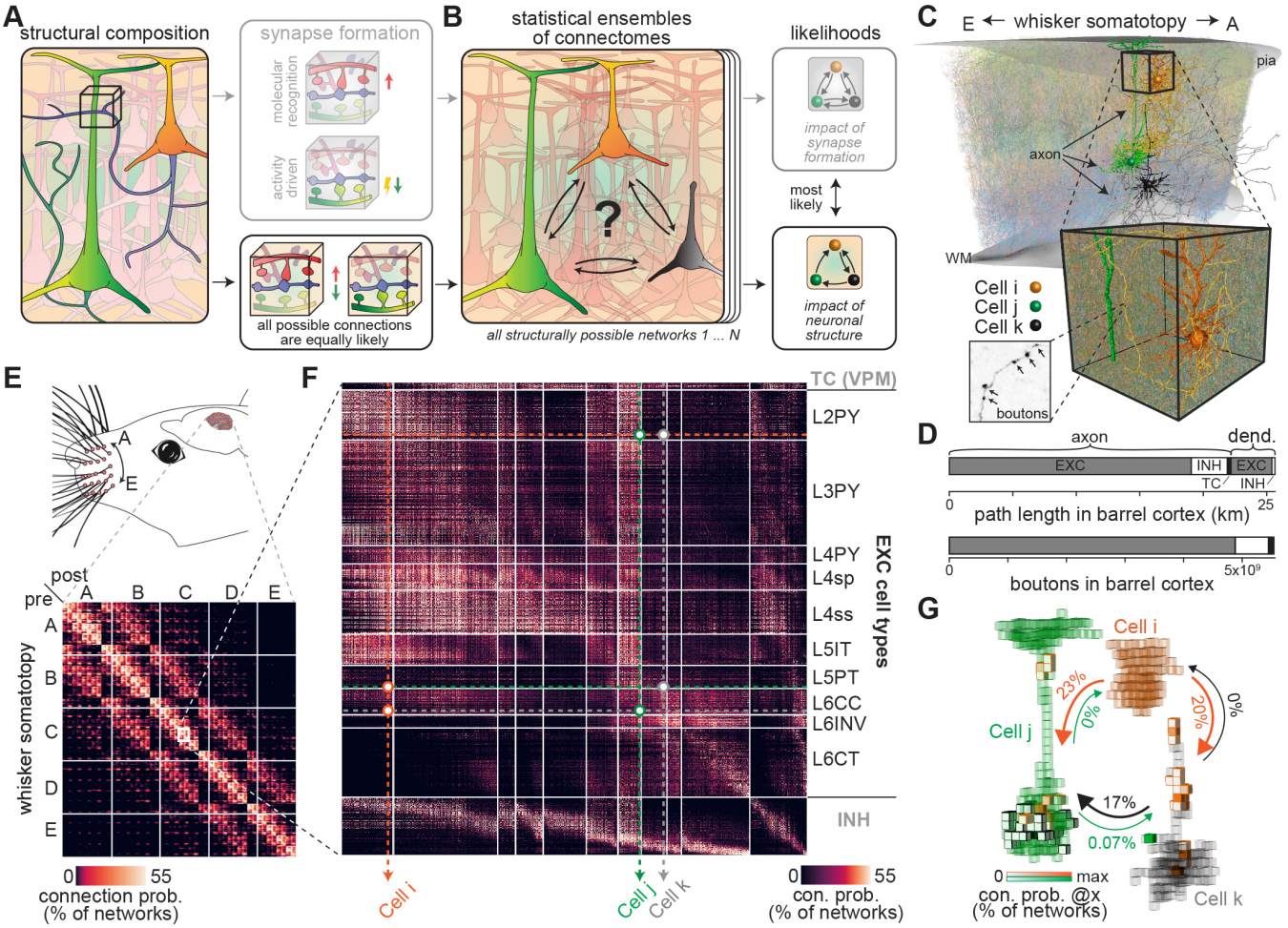

Figure 1. Concept for testing the impact of neuronal structure on cortical network architecture. **(A)** Schematic illustration: We divide dense reconstructions of the neuropil into subvolumes, count the number of pre- and postsynaptic structures along axons and dendrites, and generate different network models which can account for them. Here, each of the three axonal boutons (blue) could be connected to one of the nine spines from one of four different neurons (green, red, pink, purple), resulting in 504 different network configurations **(Fig. S1A)**. **(B)** The resulting statistical ensemble of connectomes allows us to calculate how likely each of such network configurations would appear in the absence of synapse formation strategies that result in wiring specificity (e.g. molecular recognition and activity dependence). **(C)** Dense model of the structural composition for the rat barrel cortex, in which neurons are represented by *in vivo* labeled axon and dendrite morphologies, including distributions of pre- (i.e., boutons) and postsynaptic structures (e.g. spines). Inset illustrating how boutons were quantified along axons is adapted from (*19*). **(D)** Path lengths of neuronal processes and the number of synaptic structures along them (e.g. boutons) for all excitatory (EXC) and inhibitory (INH) neurons in the model, and thalamocortical (TC) axons from the ventral posterior medial nucleus (VPM). **(E)** Matrix representation of the statistical ensemble of connectomes for the volume that represents the 24 major facial whiskers (i.e., A1-E4, α-δ). Connection probabilities reflect the fraction of networks in which the respective neurons are connected. **(F)** Zoom-in to the barrel column representing the C2 whisker. The matrix is sorted by soma depth and cell type: VPM (only presynaptic), INH and EXC (subdivided into pyramidal neurons in layers 2-4 (L2PY, L3PY, L4PY), star pyramids (L4sp), spiny stellates (L4ss), intratelencephalic (L5IT), pyramidal tract (L5PT), corticocortical (L6CC), corticothalamic (L6CT) and inverted (L6INV) neurons). **(G)** Axo-dendritic overlap between the three example neurons from panel C/F (here at 50 µm resolution). Arrows denote the likelihoods that e.g. the axon of $Cell\ i$ is connected by at least one synapse to the dendrites of $Cell\ j$ within one of their overlap volumes (i.e., in 23% of the structurally possible networks).

Results

We had previously introduced a computational framework (*19*) which can transform dense reconstructions of the neuropil into a set of all structurally possible networks, and determine the likelihoods of each of those networks for a given selection of mathematically formulated wiring rules **(Fig. 1A)**. Analogous to statistical mechanics (*22*), we refer to these rule-based probability distributions of neuronal networks as 'statistical ensembles of connectomes'. Comparing statistical ensembles of connectomes that reflect different wiring rules thereby allows exploring the impact of different synapse formation strategies on neuronal network architecture. Moreover, the framework allows exploration of how the neuronal structure itself could impact network architecture **(Fig. 1B)**. This strategy is illustrated in **Figure 1A**, where a schematized subvolume comprises three boutons along one axonal branch and nine spines along the dendritic branches from four different excitatory neurons. When each of these boutons is assigned to one of the spines in its vicinity, the particular structural composition of this subvolume alone gives rise to $9!/(9-3)! = 504$ possible networks that differ in how the five neurons from which these branches originate are connected to one another **(Fig. S1A)**. Here we calculate how likely each of such structurally possible networks would occur, when synapse formation strategies that result in wiring specificity are neglected (e.g. molecular recognition and activity dependence). For this, we assume that all presynaptic boutons are equally likely to connect independently to any of the postsynaptic structures (e.g. spines) that are present within the same subvolume **(Fig. S1B)**. Statistical ensembles of connectomes based on these wiring rules hence provide the likelihoods for how neuronal networks could appear if they were solely due to the underlying structural composition of the neuropil.

Here we apply this strategy to investigate how neuronal structure impacts cortical network architecture. For this, we had previously reverse engineered the structural composition of the neuropil for the volume of rat barrel cortex that represents the 24 major facial whiskers (reviewed in (*23*)). This dense model of the spatial distributions of all neurons, and their dendrites and axons – including the distributions of pre- and postsynaptic structures along these neuronal processes **(Fig. 1C)**, is based on quantitative anatomical data that we had systematically collected during the past two decades for the rat barrel cortex and the primary thalamus of the whisker system (i.e., the ventral posterior medial nucleus (VPM)). All anatomical data originated from rats of the same strain, sacrificed at similar time points following the critical periods of neuron morphology development. The model comprises a cortical volume of 6.8 mm^3 (*24*), contains 477,551 excitatory and 69,788 inhibitory neurons, and is innervated by 6,225 neurons from VPM thalamus (*25*). These neurons give rise to 25.6 km of axonal and dendritic processes within the barrel cortex, which represent more than 5.5 billion pre- and postsynaptic structures, respectively **(Fig. 1D)**. By applying our computational framework **(Fig. S1C)**, we derived all structurally possible networks for this dense model of the rat barrel cortex, calculated how likely these networks are to appear in the absence of synapse formation strategies that introduce wiring specificity **(Fig. 1E)**, and analyzed the resulting statistical ensemble of connectomes with respect to the neurons' cell types and locations **(Fig. 1F)**. Thus, our statistical modeling approach provides quantitative predictions for how neuronal structure impacts wiring between arbitrarily grouped neurons across the rat barrel cortex, as well as for where along their dendrites and axons connections could occur **(Fig. 1G)**.

The model provides realistic estimates for the structural composition of the rat barrel cortex

To what degree our reverse engineering approach can provide realistic estimates for the structural composition of the neuropil remained so far unclear. This information is however crucial for judging the validity of the derived statistical ensembles of connectomes. Consistent with early estimates (*26*), the barrel cortex model predicts that 3.3 km of axons and 0.5 km of dendrites are compressed into each cubic millimeter of cortical tissue **(Fig. 2A)**. Such high packing densities represent a major challenge for dense electron microscopic reconstructions (*27*). The largest densely reconstructed cortical volume hence comprises only ~500,000 μm^3 (*13*). However, this remarkable effort in layer 4 of mouse barrel cortex had

provided first quantitative data about the structural composition of the cortical neuropil, and revealed that volumes with such dimensions **(Fig. 2B)** can comprise more than 45,000 neuronal processes, which represent ~2.7 m of path length and ~400,000 synaptic connections. These empirical observations fall well within the respective ranges predicted by the model **(Fig. 2C)**. Consequently, the structurally possible configurations by which neuronal processes could be connected locally to one another in the model of rat barrel cortex (i.e., within subvolumes <500,000 µm^3) will be qualitatively and quantitatively very similar to those that could emerge from the densely reconstructed volume of mouse barrel cortex. Also consistent with the empirical data, the model predicts that more than 97% of the neuronal processes remain unconnected to a soma that lies within the same subvolume. The model thereby provides first insight into the diversity of the cellular and cell type origins for all unconnected neuronal processes within cortical subvolumes **(Fig. 2D)**.

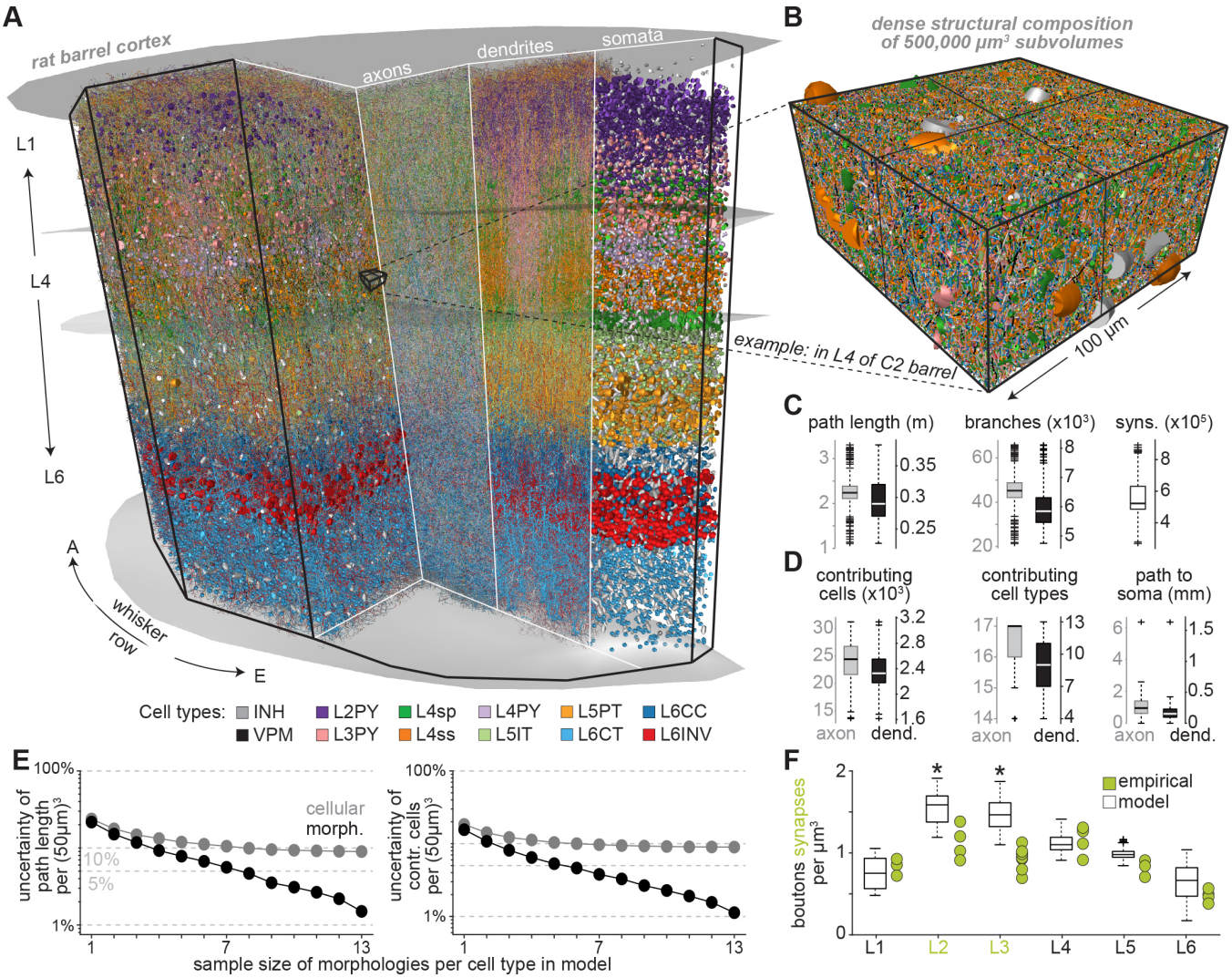

Figure 2. Validation of the dense structural model of rat barrel cortex. (A) Cross-section through the barrel cortex model, illustrating the dense distributions of somata, dendrites and axons (fractions shown), colored by their respective cell types. **(B)** Zoom-in shows one example subvolume, whose dimensions and location resemble that of the largest densely reconstructed dataset reported so far (*13*). **(C)** Path lengths, the corresponding numbers of branches, and the synaptic structures that they represent, for axons (grey) and dendrites (black) within 500,000 µm^3 large subvolumes (n=128) across the model. **(D)** Branches that are unconnected to a soma within the same subvolume (>97%) originate from >25,000 neurons (left), which reflect a diverse range of cell types (center), and whose somata are ~0.9 mm away

(right). The 17 cell types reflect VPM, INH (subdivided by layers 1-6) and EXC neurons (subdivided as in panel A). **(E)** Quantification how robustly our reverse engineering approach can predict the structural composition of each subvolume within the rat barrel cortex (see also **Fig. S3C**). Left: robustness of the packing density of neuronal processes for each subvolume depending on the number of morphologies per cell type that was used to generate the model **(Fig. S2)**. Black markers represent the coefficients of variation (CVs) in path length per subvolume across >30,000 models (i.e., median across 125,000 μm^3 large subvolumes), where all models are based on the same average soma distribution (*25*). Grey markers represent the median CVs for the same subvolumes across models that were based on different empirically measured soma distributions. Right: same robustness analysis for the numbers of neurons from which these processes originate. **(F)** Predicted bouton densities per layer versus synapse densities measurements in juvenile rats (*28*). The differences in layers 2/3 (L2/3) between the model and the empirical data (denoted by asterisks) likely reflect age differences (i.e., the data for the model was acquired after postnatal day P28, the empirical data at P14). Synapse densities increase particularly in the upper layers after P14 (*29*).

The model predicts for both the amount of neuronal processes and the number of synaptic structures that they represent substantial variations across the different subvolumes of the barrel cortex **(Fig. 2C/D)**. We therefore tested whether these variations of the structural composition are anatomically realistic. For this, we reanalyzed our previously reported anatomical data **(Fig. S2)** and systematically quantified the variability of neuron soma, dendrite and axon distributions across the barrel cortex, as well as across animals **(Fig. S3A/B)**. We captured the hereby quantified cellular and morphological variability by repeating the reverse engineering approach to generate >30,000 barrel cortex models, which reflected different measured soma distributions and/or samples of *in vivo* labeled dendrite and axon morphologies. This revealed that the structural composition of each subvolume within the barrel cortex model would not change by more than 12% – the diversity of the cellular origins of neuronal processes by no more than 8% – even if the model was based on a larger sample of reconstructed morphologies **(Fig. 2E)**. Moreover, the model predicts layer-specific density variations of synaptic structures **(Fig. 2F)** that are consistent with electron tomography measurements in the barrel cortex of juvenile rats (*28*). Thus, our model provides realistic and robust estimates for the amounts of axonal and dendritic branches within any subvolume of the rat barrel cortex, for the synaptic structures that these processes represent, and for the diversity of their respective cellular and cell type origins **(Fig. S3C)**. Consequently, the model-derived statistical ensemble of connectomes yields valid, quantitative predictions for how neuronal networks could appear in barrel cortex if they were solely due to the structural composition of its neuropil.

Cortical networks cannot be consistent with Peters' Rule

We used the statistical ensemble of connectomes to test whether the absence of synapse formation strategies that introduce wiring specify would result in neuronal networks that obey Peters' Rule. For this, we determined the axo-dendritic overlap at different spatial resolutions (here: cubic volumes with 1, 5, 10, 25, 50 or 100 µm edge lengths) for all neuron pairs in the model and quantified the respective amounts of synaptic structures that these neuronal processes represent within each overlap volume **(Fig. 3A)**. We illustrate these quantifications for one example subvolume at the resolution of 50 µm, which contains more than 23,000 axonal and 2,200 dendritic branches that represent more than 100,000 boutons (PREs) and postsynaptic structures (POSTs), respectively **(Fig. 3B)**. When each of these boutons is assigned to one of the postsynaptic structures, the composition of this particular subvolume alone gives rise to an enormous number of structurally possible networks that differ in how the ~15,000 neurons from which these neuronal processes originate are interconnected **(Fig. S1B)**. In the vast majority of these networks, the axons and dendrites of any particular neuron pair remain unconnected – i.e., their pre- and postsynaptic structures connect to those of other neurons that overlap in this subvolume **(Fig. 3C)**. Thus, axo-dendritic overlap can in principle predict connectivity for only a small minority of overlapping branch pairs. Moreover, most neurons contribute more than one synaptic structure to this subvolume, which

results in configurations where axon-dendrite pairs are interconnected by several synapses **(Fig. 3D)**. In any of the structurally possible networks and across all subvolumes, 99.6 ± 0.1% of the axon-dendrite pairs remain unconnected despite their overlap, while a substantial fraction of them forms synaptic clusters of up to five connections – and of even more in some subvolumes. These violations of Peters' Rule are a direct consequence of the high packing density of neuronal processes, which leads to a number of axon-dendrite pairs that exceeds the number of synaptic structures that they represent by one to two orders of magnitude, irrespective of the spatial resolution at which overlap is determined **(Fig. 3E)**.

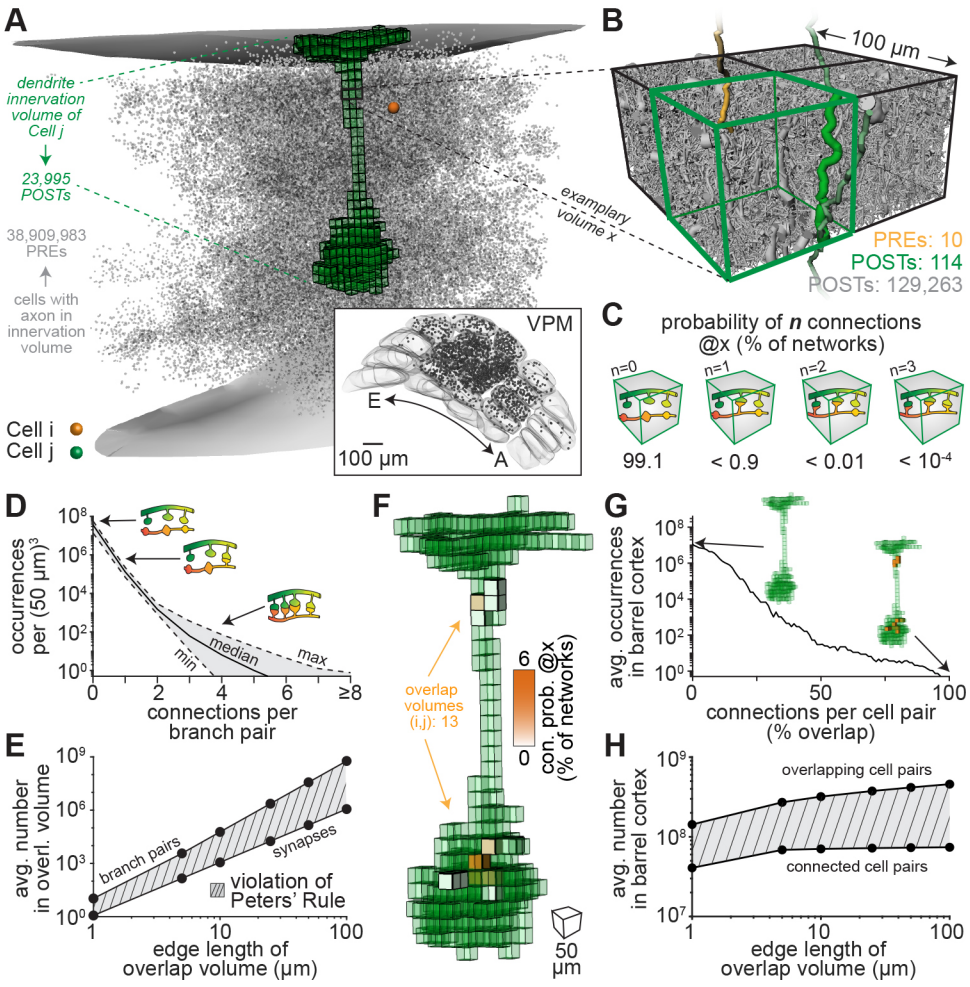

Figure 3. Testing of Peters' Rule. (A) Neurons (grey, 50% shown) in barrel cortex and VPM whose axons overlap with the dendrites of the L5PT from **Fig. 1C** (green) at a resolution of 50 µm. The orange marker represents the soma of the L2PY from **Fig. 1C**. **(B)** Example subvolume in which the L2PY axon represents ten presynaptic structures (PREs; i.e., boutons). The L5PT dendrites represent 114 postsynaptic structures (POSTs; i.e., spines). The number of 129,263 POSTs reflects all spines in this subvolume, as well as target sites on the surfaces of inhibitory somata and dendrites **(Fig. S1B)**. **(C)** Probabilities that none, one or more of the pre- and postsynaptic structures of the L2PY and L5PT are connected **(Fig. S1C)**. **(D)** Axon-dendrite pairs whose overlap at 50 µm resolution yields none, one or more connections across all possible networks. **(E)** Overlapping branch pairs versus the synaptic structures that they represent for different resolutions at which axo-dendritic overlap is determined. If Peters' Rule were true, the two lines should match. **(F)** At 50 µm resolution, the L2PY axon overlaps with the L5PT dendrites in 13 subvolumes. **(G)** Overlap volumes for all neuron pairs versus connections between them. 100% indicates that two neurons are connected by as many synapses as they have overlap volumes. **(H)** Neuron pairs that overlap versus connected neurons across all possible networks.

The violations of Peters' Rule become even more severe at cellular scales. The axons and dendrites of neuron pairs typically overlap in more than one subvolume **(Fig. 3F)**. The probability that overlap translates into connectivity is already very low within each individual subvolume. The likelihood that networks occur in which any particular neuron pair is interconnected in all of its overlap volumes is hence in general infinitesimally small **(Fig. 3G)**. Irrespective of the spatial resolution at which overlap is determined, a vast majority of neurons whose axons and dendrites overlap will remain unconnected in any of the networks that could emerge from the structural composition of the rat barrel cortex **(Fig. 3H)**. Consequently, testing the validity of Peters' Rule is not equivalent to testing the impact of neuronal structure on network architecture. Thus, empirical observations that falsify Peters' Rule do in general not provide insight into the underlying synapse formation strategies, and in particular do not justify conclusions that these neurons must have been interconnected based on their cellular identity or activity.

Wiring specificity at synaptic levels is not required for nonrandom network formation

Next, we tested whether the absence of synapse formation strategies that introduce wiring specify would result in random networks. For this, we compared the topological properties of the structurally possible networks in barrel cortex with those of randomly connected networks that have the same underlying pairwise statistics. More specifically, we calculated the respective occurrences of the possible wiring patterns by which three neurons could be connected to one another – commonly referred to as triplet motifs **(Fig. 4A)**. The likelihood that three neurons in the barrel cortex model form a particular motif depends on their respective pairwise connection probabilities in the statistical ensemble of connectomes. For example, the three neurons shown in **Figure 1G** will most likely form the motif with a single unidirectional connection (i.e., L2PY → L5PT), less likely motifs with one bidirectional connection (i.e., L5PT ←→ L6CC), and never motifs with more than one bidirectional connection (i.e., the L5PT and L6CC axons do not overlap with the L2PY dendrites). Consequently, the motifs that are formed by any particular subset of neurons will differ across the different structurally possible networks **(Fig. 4B)**. However, in any structurally possible network, we found that the respective occurrences of motifs deviate in general from those of random networks **(Fig. 4C)**, despite the fact that both the barrel cortex and the random networks are based on the same pairwise connection probability distributions **(Fig. 4D)**.

The degrees to which the occurrences of motifs differ from those of random networks depended on how we grouped neurons in the barrel cortex model. For example, while feedforward loops (motif 7) occur more frequently in the barrel cortex model than in random networks (i.e., overrepresented), they are underrepresented in the subnetworks formed by excitatory neurons in layer 5 **(Fig. 4E)**. In general, the respective occurrences of any of the triplet motifs changed depending on how we grouped neurons with respect to layer, barrel column, cell type, inter-somatic distance, or combinations thereof **(Fig. S4)**. Interestingly, these grouping-specific occurrences of motifs correlated with differences in the shapes of the underlying pairwise statistics. For example, the occurrences of the recurrent feedforward motif (motif 10) transition from over- to underrepresentation depending on the respective means of the connection probability distributions **(Fig. 4F)**. Moreover, the magnitude of over- and underrepresentation increases with increasing and decreasing widths of the connection probability distributions, respectively. These relationships indicate that the mean and the coefficient of variation (CV) of connection probabilities – in the following referred to as the degrees of network sparsity and heterogeneity – can quantitatively and qualitatively impact the nonrandom topological properties of neuronal networks. Beyond triplet motifs, strong degrees of recurrence characterize the structurally possible networks, as overrepresentation increases with the number of bidirectional connections and with the number of neurons per motif **(Fig. 4G)**. Conversely, underrepresentation of feedforward motifs increases with the number of neurons per motif. Consequently, the topology of cortical networks will deviate in general from those of random networks, even if synapse formation strategies that introduce wiring specificity were absent. Thus, empirically observed nonrandom motif occurrences do not provide insight into the underlying synapse formation strategies, and do not justify conclusions that such patterns must reflect a particular wiring rule.

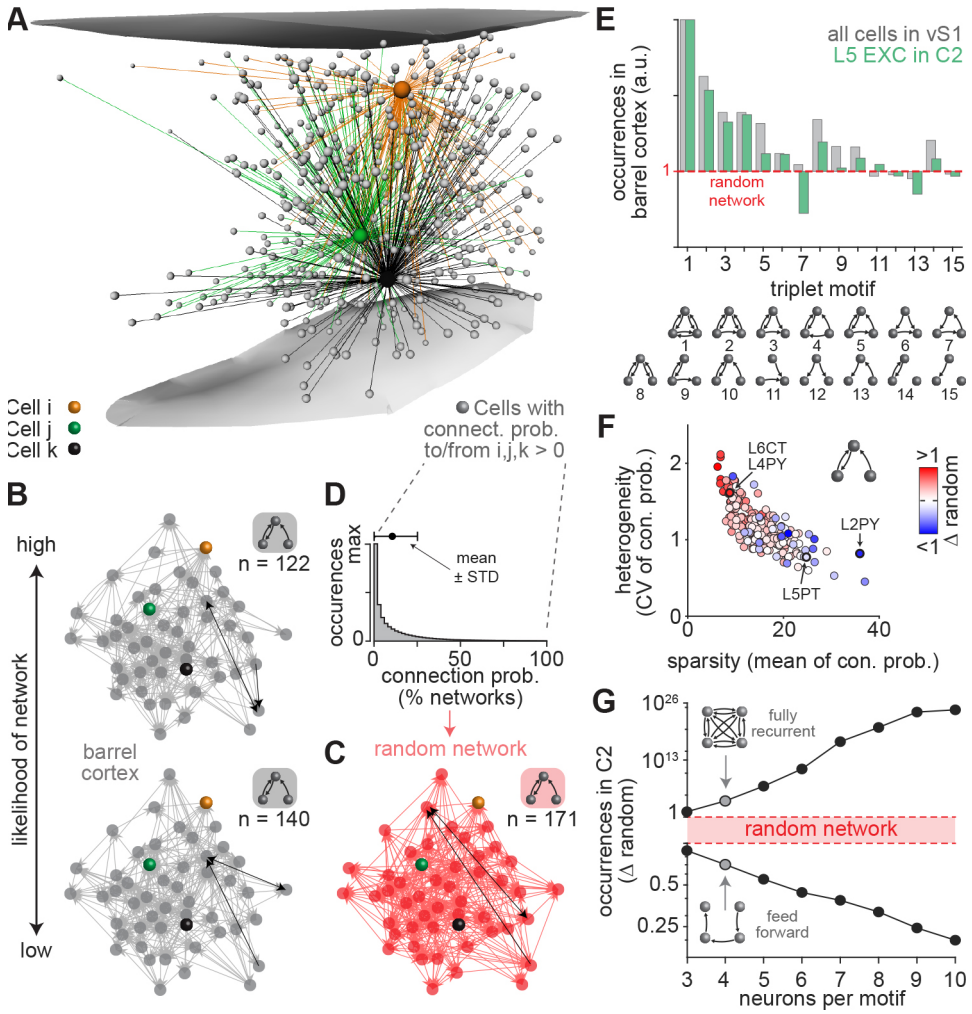

Figure 4. Structurally determined topological properties of cortical networks. (A) Somata of neurons (grey, 0.1% shown) whose axons overlap with the dendrites of one of the neurons from **Fig. 1G**. **(B)** Two possible network configurations for 50 neurons from panel A that are predicted to occur with different likelihoods from the structural composition of the barrel cortex model. **(C)** Random network example derived from the same pairwise connection probability distribution that was used to generate the networks in panel B. The number of nodes and edges are identical to panel B, but the occurrences (n) of motifs differ (e.g. motif 10 in panel E). One motif 10 is highlight in black per network in panels B/C. **(D)** Connection probability distribution for all pairs of neurons from panel A. **(E)** Ratios between motif occurrences in networks derived from the model versus random networks (1: equally abundant; >1: overrepresented in the model; <1: underrepresented). **(F)** Deviations in the occurrences of motif 10 between the model and random networks for different cell type-specific groupings (n=220) versus the respective means and CVs of the underlying connection probability distributions. **(G)** The likelihoods to observe recurrent loops and feedforward chains between up to ten neurons in networks predicted by the structural composition of barrel cortex versus in random networks.

Structural basis of nonrandom networks

How is it possible that neuronal structure translates into nonrandom network architectures? How can the degrees of sparsity and heterogeneity in pairwise connectivity have such a defining impact on the networks' specific nonrandom topological properties? To address these questions, we systematically explored the mathematical foundations that underlie the occurrences of network motifs. For this, we consider our statistical ensemble of connectomes as a distribution of pairwise connection probabilities that generates network configurations. If each of the connections is drawn independently from any such generating distribution, motifs will occur as expected for randomly connected networks – i.e., occurrences are independent from the network's heterogeneity and only reflect the mean of the underlying pairwise statistics **(Fig. 5A**; see Equation S1 in the **Supplementary Materials**). Thus, our observations of nonrandom occurrences of motifs, and their dependencies on network heterogeneity, cannot be consistent with the assumption that connection probabilities are independent of one another. Instead, only correlations in the statistical ensemble of connectomes could explain our observations **(Fig. 5B)**.

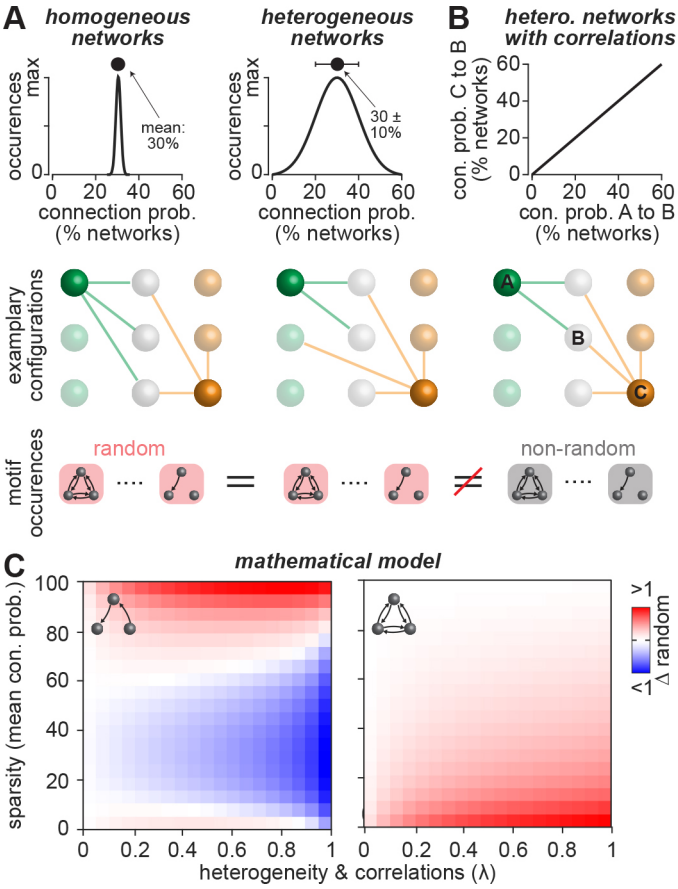

Figure 5. Mathematical foundations for nonrandom motif occurrences. (A) Toy example illustrating Eq. S1 in the **Supplementary Materials**. Left: Statistical ensembles of connectomes that yield homogeneous pairwise connectivity (i.e., standard deviation << mean) will result in networks where all nodes have mostly the same number of edges (here illustrated by two nodes that both have three edges). Right: statistical ensembles of connectomes that yield heterogeneous pairwise connectivity (i.e., standard deviation ≈ mean) will result in networks where the nodes have on average the same number of edges. Bottom panels: occurrences of triplet motifs will be on average random and identical in all networks that have the same mean connection probability. **(B)** Toy example illustrating Eq. S2-3 in the **Supplementary Materials**. Statistical ensembles of connectomes that yield correlations in pairwise connectivity (here illustrated by two nodes that both connect to the same nodes) will result in motif occurrences that deviate from those of random networks. **(C)** A mathematical model **(see Supplementary Materials)** that represents statistical ensembles of connectomes with correlations reveals how the mean (i.e., sparsity) and width (i.e., heterogeneity) of pairwise connectivity impact nonrandom motif occurrences; here illustrated for feedforward chains (left) and recurrent loops (right).

We therefore investigated how the presence of correlations affects the occurrences of motifs. For this, we developed a mathematical model, which assumes that each connection derived from the statistical ensemble of connectomes reflects a 'private' and a 'shared' source (*30*). The bigger the shared source relative to the private one, the more correlated are the connection probabilities. For simplicity, we assume here that correlations and heterogeneity are expressed by single parameter λ. A comprehensive description of the mathematical model is provided in the **Supplementary Materials**. The mathematical model yields motif occurrences that match those in random networks only when correlations are absent (i.e., $\lambda = 0$; see Equation S2-3 in the **Supplementary Materials**). In turn, for statistical ensembles of connectomes with correlations, the mathematical model allows exploring how sparsity and heterogeneity

in pairwise connectivity will generally affect nonrandom motif occurrences. For example, in sparsely connected networks (e.g. mean connection probability of 10%) feedforward motifs become increasingly underrepresented with increasing heterogeneity **(Fig. 5C)**. Conversely, in densely connected networks (e.g. mean of 90%) such motifs become increasingly overrepresented with increasing heterogeneity. Recurrent loops are always overrepresented in the presence of correlations, and overrepresentation increases the sparser and the more heterogeneous a network is interconnected.

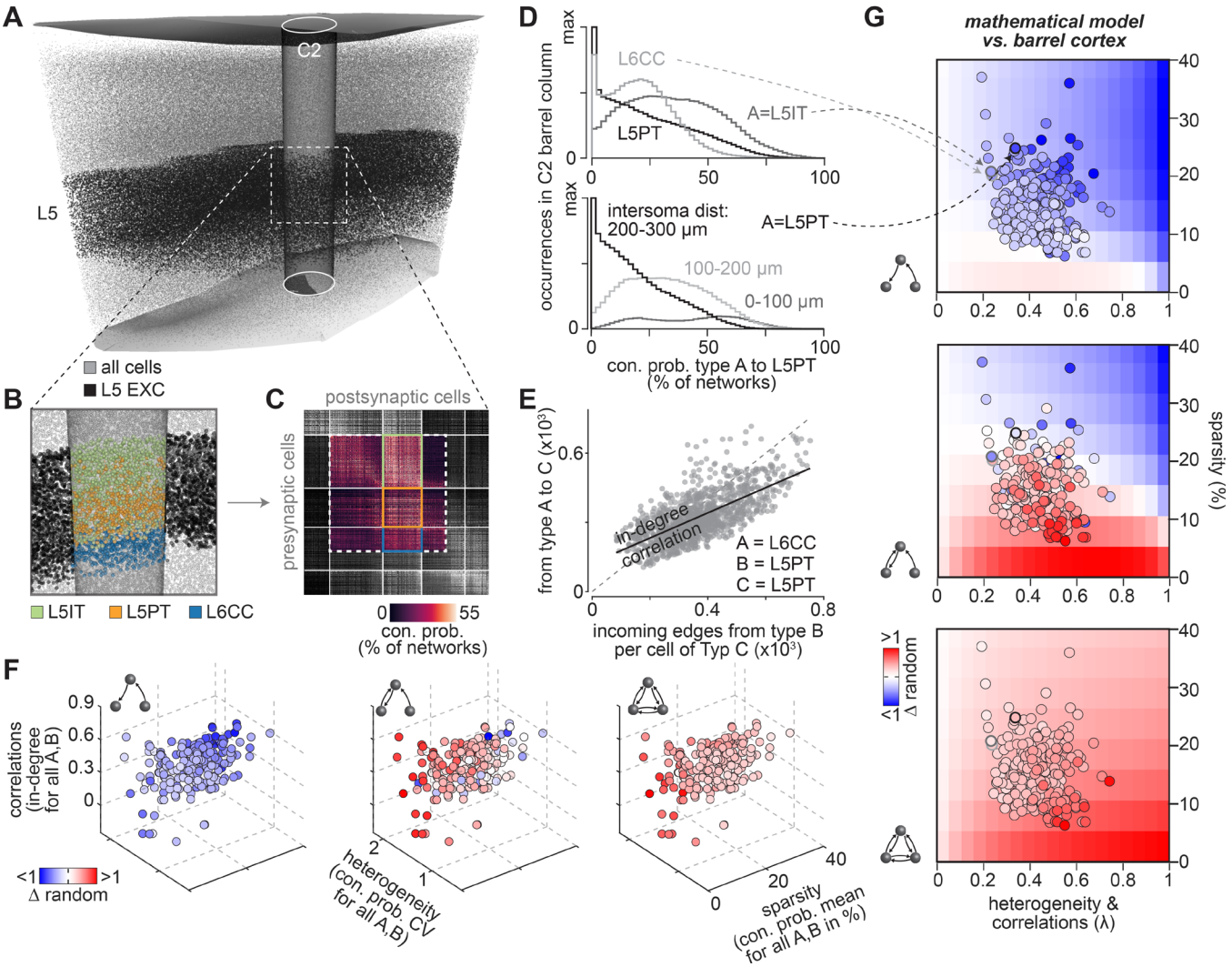

Figure 6. Structural determinants for nonrandom motif occurrences in cortical networks. (A) The impact of neuronal structure on connectivity is illustrated for EXC neurons in layer 5 of the C2 barrel column. **(B)** Zoom-in shows somata colored by their respective cell type. **(C)** Part of the matrix representation of the statistical ensemble of connectomes from **Fig. 1F** that represents the neurons shown in panel B. **(D)** Distributions of connection probabilities from the matrix in panel C for different cell type combinations. Bottom panel: connection probability distributions between L5PTs for different inter-somatic distances. **(E)** In-degree distributions derived from the matrix in panel C. The numbers of incoming connections that L5PTs receive from one another correlates with those they receive from L6CCs. **(F)** Motif occurrences in the barrel cortex model versus those in random networks depend on the in-degree correlation coefficients, the means and CVs of the corresponding connection probability distributions for more than 200 groupings that represent neurons with different cell types. **(G)** Nonrandom motif occurrences for the groupings in panel F are consistent with the mathematical model.

We tested whether correlations, in conjunction with sparsity and heterogeneity, could indeed explain our observation that the structural composition of the neuropil results in nonrandom network architectures. We illustrate these quantifications for excitatory neurons in layer 5 **(Fig. 6A)**. About 80% of these neurons represent either intratelencephalic (L5ITs), pyramidal tract (L5PTs) or corticocortical neurons (L6CCs) **(Fig. 6B)**. We therefore analyzed the pairwise statistics with respect to these morphological cell types by grouping the connection probability values in the statistical ensemble of connectomes accordingly **(Fig. 6C)**. Even though neuron somata from all of these cell types intermingle, the shapes of the respective connection probability distributions differ substantially. For example, L5ITs are predicted to connect more densely and less heterogeneously to L5PTs than L5PTs connect to one another **(Fig. 6D)**. Within the population of L5PTs, the shapes of connection probability distributions differ substantially depending on how far apart their somata are **(Fig. 6D)**. Thus, in any network that could emerge from the statistical ensemble of connectomes, the degrees of sparsity and heterogeneity in pairwise connectivity will reflect the locations of neurons and their respective morphological properties **(Fig. S5)**.

Similarly, the shapes of degree distributions depended on the grouping of neurons by their respective locations and morphological cell types **(Fig. S5)**. Plotting degree distributions jointly for different groupings revealed the presence of substantial correlations in pairwise connectivity within the statistical ensemble of connectomes. For example, L5PTs are predicted to receive more connections from one another the more connections they receive from L6CCs **(Fig. 6E)**. These in-degree correlations reflect similarities in axon projection patterns. More specifically, despite substantial quantitative and qualitative morphological differences between L5PTs and L6CCs, the axons of both populations predominantly innervate the deep layers, where they span horizontally across several barrel columns (*31*). In contrast, L5IT axons predominately innervate the upper layers and remain largely confined to the dimensions of a single barrel column in the deep layers. As a result, in-degree correlations are much weaker between L5ITs and the other two cell types **(Fig. S5)**. Thus, correlations in pairwise connectivity will be present in any structurally possible network, and the strengths of these correlations will reflect similarities in the neurons' locations and their respective morphologies.

These observations generalize beyond the example of excitatory neurons in layer 5. We illustrate this by calculating the correlation coefficients between degree distributions, as well as the means and CVs of the corresponding connection probability distributions, for more than 200 groupings that represent neurons with different cell types. For any of the groupings, motif occurrences deviated from those of random networks **(Fig. 6F)**. More specifically, the sparser and the more heterogeneous neurons are interconnected within a particular group, the more overrepresented are recurrent connections between them. Conversely, the more densely the group is interconnected, the more underrepresented are feedforward connections. These relationships are consistent with the mathematical model **(Fig. 6G)**. Thus, the shapes and correlations of pairwise connectivity statistics that solely reflect the structural composition of the underlying neuropil represent a defining source of nonrandom network architectures, whose specific topological properties hence reflect the morphological properties of their constituents.

Neuronal structure predicts empirically observed wiring specificity

The statistical ensemble of connectomes revealed four principles by which neuronal structure impacts network architecture. First, because of the mismatch between synaptic structures and branch pairs, the vast majority of neurons whose axons and dendrites overlap remain unconnected. As a result, the higher the packing density of neuronal processes, the smaller the probability that their respective pre- and postsynaptic structures could be connected to one another. Thus, packing density translates into the means of connection probability distributions, and thereby defines a networks' sparsity **(Fig. 7A)**. Second, the higher the cellular diversity of neuronal processes that overlap – e.g. with respect to the morphological cell types of the neurons that these processes belong to – the broader the shapes of connection probability distributions when neurons are grouped by these cellular features. Thus, cellular diversity translates into the widths of connection probability distributions, and thereby defines a network's

heterogeneity **(Fig. 7B)**. Third, the more similar the dendrite or axon projection patterns of neurons are, the more similar are their respective contributions to the packing density and cellular diversity of neuronal processes across subvolumes. Thus, similarities in the neurons' locations and morphologies translate into correlations **(Fig. 7C)**. Fourth, in the presence of correlations, the degrees of sparsity and heterogeneity define a network's specific nonrandom topology. The high packing density and cellular diversity of the cortex thereby yield nonrandom recurrent network architectures **(Fig. 7D)**. Tissue with low packing density and cellular diversity yields feedforward architectures.

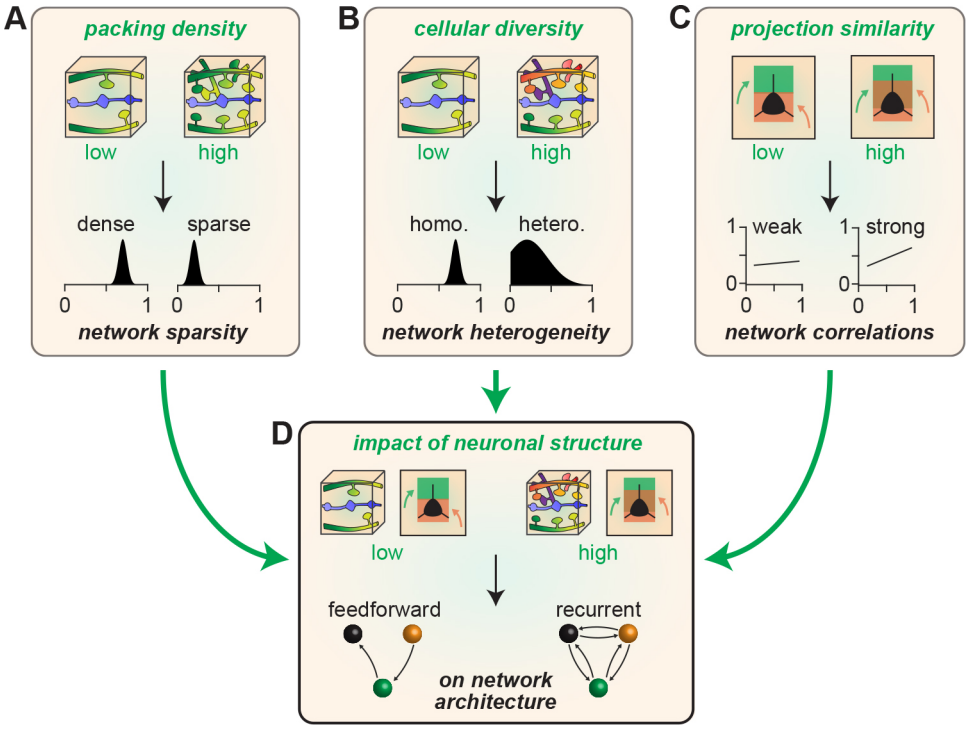

Figure 7. The impact of neuronal structure on network architecture. (A) The packing density of neuronal processes translates into the means of connection probability distributions, and thereby defines a networks' sparsity. **(B)** The cellular diversity of neuronal processes that overlap – e.g. with respect to cell type – translates into the widths of connection probability distributions, and thereby defines a network's heterogeneity. **(C)** Similarities in the dendrite or axon projection patterns of neurons translate into correlations of connection probability and degree distributions. **(D)** In the presence of correlations, the degrees of sparsity and heterogeneity define a network's specific nonrandom topology. Feedforward motifs become increasingly overrepresented the denser and the more homogeneously neurons are interconnected (i.e., low packing density and low cellular diversity). Conversely, recurrent motifs become increasingly overrepresented the sparser and the more heterogeneously neurons are interconnected.

How strong is the impact of neuronal structure on network architecture compared to that of synapse formation strategies that introduce wiring specificity? Here we can address this question, because the present statistical ensemble of connectomes provides a proper null hypothesis for testing to what degree empirically observed wiring specify in barrel cortex could reflect the structural composition of the neuropil, or whether it must be due synapse formation strategies that interconnect neurons based on their activity or cellular identity. For this, we compared our model with a rich body of literature that represents several decades of quantitative connectivity measurements by many different laboratories and by a variety of experimental techniques. First, we tested whether the predicted relationship between packing density and sparsity in pairwise connectivity is observed empirically. For example, 500,000 μm^3 subvolumes in layer 4 of the model comprise on average more than 10^8 axon-dendrite pairs. In any of the structurally possible networks, the vast majority of these branch pairs will remain unconnected **(Fig. 8A)**, while ~10^5 are predicted to be connected by a single synapse, ~4,000 by two synapses, ~150 by three synapses

and ~20 by four or more synapses **(Fig. 8B)**. These predictions for both the packing density and the resulting degrees of sparsity are virtually indistinguishable from those observed empirically via dense reconstructions in mouse barrel cortex (*12, 13*).

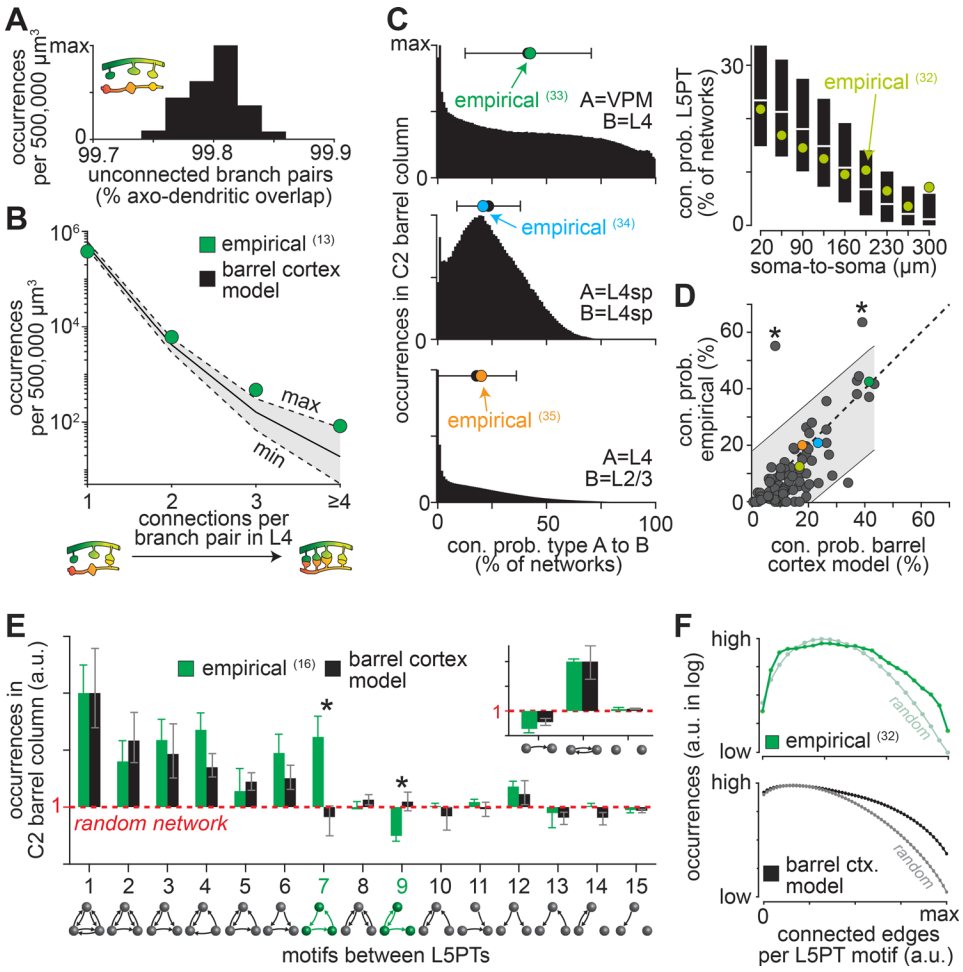

Figure 8. Predicted versus empirical connectivity data. (A) Occurrences of unconnected branch pairs per 500,000 µm³ large subvolumes in layer 4 of the model (n=252). **(B)** Occurrences of branch pairs connected by one or more synapses for the same subvolumes as in panel A match with empirical data from mouse barrel cortex (*13*). **(C)** Predicted connection probabilities match those of four example studies (*32-35*). **(D)** Empirical connection probabilities for 89 layer and/or cell type groupings versus those predicted by the model **(Tables S1-3)**. Grey shading represents 95% prediction interval. Asterisks denote inconsistencies with empirical data. **(E)** Ratios of L5PT motif occurrences in the model match empirical data (*16*). Y-axis in log scale. Error bars represent standard deviations estimated by bootstrap method for empirical data, and range across models for model data (**Fig. S6**). **(F)** Overrepresentation of motifs between eight L5PTs increases with the number of connected edges empirically (*32*) and in the model (bottom panel). Y-axis in log scale.

Second, we tested whether the predicted relationship between cellular diversity and heterogeneity in pairwise connectivity is observed empirically. For this, we made groupings of neurons in the barrel cortex model analogous to those reported by sparse measurements of pairwise connectivity that sampled neurons depending on their soma locations within a particular layer, cell types, inter-somatic distances, or combinations thereof **(Fig. 8C)**. In total, we predicted the pairwise connectivity for eighty-nine such samplings that reflect different cellular properties, and compared those with the respective empirical data reported across a set of twenty-nine studies **(Tables S1-3, Fig. S6)**. The predicted connection probabilities correlated significantly with the empirical data ($R=0.75$, $p<10^{-16}$). About 2/3 of the empirically

determined connectivity values deviated from the prediction by less than half a standard deviation of the respective connection probability distribution, 94% by less than one standard deviation **(Fig. 8D)**. To test whether this consistency emerges by chance, we performed random permutations of the eighty-nine predicted connection probabilities. Permutations yielded correlations with the empirical data that were not significant (R=0.00 ± 0.11).

Finally, we tested whether the predicted nonrandom occurrences of motifs are observed empirically. The occurrences of all fifteen triplet motifs and their respective deviations from a random network were systematically assessed for L5PTs (*16*). The statistical ensemble of connectomes predicts motif occurrences for this cell type that are remarkably consistent with these empirical data, with the notable exception of the feedforward loop and the recurrent feedback motif **(Fig. 8E)**. Moreover, probing the occurrences of motifs between up to eight L5PTs revealed that independent of their particular topology, motifs become increasingly overrepresented with increasing numbers of connected edges (*32*). This relationship is qualitatively consistent with our predictions **(Fig. 8F)**. Thus, wiring specificity from subcellular to network scales that was observed empirically between excitatory neurons – i.e., the occurrences of synaptic clusters; layer-, cell type- and distance-specific connectivity; over- or underrepresentation of motifs – could reflect the specific structural composition of the neuropil.

Discussion

We introduce the concept of statistical ensembles of connectomes to quantitatively test the impact of neuronal structure on cortical network architecture. We apply this strategy to an anatomically detailed model of the rat barrel cortex, which we show provides realistic and robust estimates for the dense structural composition of this entire brain area. We found that none of the structurally possible networks that could emerge in barrel cortex would be random or consistent with Peters' Rule – two observations so far considered as evidence for synapse formation strategies that interconnect neurons based on their activity or cellular identity. We reveal that these nonrandom properties reflect three factors of the neuronal structure – packing density, diversity and similarity of the neurons' processes – which will in general impact the networks' sparsity, heterogeneity, correlations and topology. Thus, unlike the assumption by Peters' Rule, we demonstrate that the impact of neuronal structure on network architecture cannot be direct in that it predicts connectivity. Instead, the impact of neuronal structure reflects properties of the pairwise and higher-order connectivity statistics that are shared by all structurally possible networks, irrespective of which particular neuron pairs whose axons and dendrites overlap are interconnected.

We emphasize that the impact of neuronal structure on network architecture does not imply that the impact of synapse formation strategies on wiring specificity is negligible (e.g. see motifs 7 and 9 in **Figure 8E**). For inhibitory neurons in particular, such conclusions are not justified. Depending on their cell type, axons of inhibitory neurons preferentially target specific other cell types and specific subcellular compartments of excitatory neurons (reviewed in (*36*)). Neuronal structure can hence be predictive for excitatory, but in general not for inhibitory connections (*13*). Interestingly, recent studies revealed that inhibitory neurons can adapt their morphologies to the specific columnar and laminar layout of a cortical area (*37, 38*). Incorporating the target specificity of inhibitory cell types into the wiring rules would hence result in statistical ensembles of connectomes that could reveal the impact of these area-specific variations of inhibitory morphologies on network architecture. For now, relationships between morphology and target specificity of inhibitory neurons are however not fully resolved. Thus, we have limited our analyses to excitatory intracortical and long-range thalamocortical connections for which empirical connectivity data is accessible.

Surprisingly, for these excitatory connections, we found that neuronal networks, which solely reflect the structural composition of the barrel cortex, predict connectivity patterns that are remarkably consistent with those observed empirically. This raises the question which synapse formation strategies could implement such strong relationships between neuronal structure and network architecture. Here, the

statistical ensemble of connectomes was based on wiring rules that are consistent with synapse formation strategies where axons compete with one another to connect to the available postsynaptic structures. Such mechanisms represent a dominating strategy for wiring up the peripheral (*39, 40*) and central nervous system (e.g. (*41*)) during development. It is hence tempting to speculate that neuron morphology development, in conjunction with competitive synapse formation strategies, establishes a scaffolding of wiring properties that defines a network's architecture. If this were true, the impact of neuronal structure on cortical network architecture may degrade throughout life. Consistency with the empirical data could thereby reflect the fact that connectivity measurements in the literature originated from rather young animals. In support of this interpretation are recent dense reconstructions of the nematode C. elegans, which revealed that the structural composition of its nervous system provides a constant scaffolding upon which connectivity is remodeled from birth to adulthood (*42*). Interestingly, some structurally determined wiring properties were maintained throughout life. This may also apply to cortex, because its proper function depends critically on the degrees of heterogeneity and correlations in connectivity (*43*) – two network properties that we show are strongly impacted by the neuronal structure. Consequently, to ensure robustness of cortical dynamics throughout life, homeostatic wiring mechanisms may maintain these structurally defined wiring properties despite the constant remodeling of cortical networks. Our statistical modelling approach provides a methodological framework for testing whether the impact of neuronal structure on cortical network architecture degrades or is maintained during maturation.

Scaffoldings of wiring properties that emerge in cortical networks during development were recently speculated to reflect an evolutionary strategy for implementing innate sensory representations and behaviors, which could facilitate learning (*44*). What exactly genomes specify about wiring remains however unknown. In C. elegans, the genome could have the capacity to specify every connection between every neuron with minute detail. In contrast, cortical synapses cannot be specified so precisely, even if the entire genome would solely encode for connections. Due to this 'genomic bottleneck', it was suggested that scaffoldings in cortical networks must be compressed within the genome via wiring rules (*44*). However, we show that the emergence of scaffoldings in networks does not rely on such explicitly encoded wiring rules. Instead, scaffoldings could be encoded implicitly via genetically induced developmental programs that guide neurons and their processes into specific subvolumes of the cortical sheet (*45*). Compared to explicit wiring rules, implicit encoding would not only solve the issue of compression through the genomic bottleneck. It may also explain how cortical networks adapt to environmental changes. More specifically, periphery-driven activity can regulate guidance programs that shape the structural composition of cortex (*46*). Accordingly, sensory experience could alter how neuronal structure impacts cortical network architecture. Implicit encoding of wiring properties via the development of neuronal structure may hence reflect an efficient evolutionary strategy that can transfer cortical network architectures across generations, while providing sufficient flexibility for invading new ecological niches (*47*).

Materials and Methods

All relevant data and codes are available from the authors. We used custom-written routines in C++, Python, or MATLAB 2020b software (Mathworks, Natick, MA, USA) for analysis and Amira software for visualization. Boxplots were generated with the Matlab built-ins *boxplot* or *boxchart* where the bottom and top of the box represents the 25th and 75th percentiles, and the line within the box the median. The lines extend to the adjacent values. Outliers are all values more than 1.5 times the interquartile range away from the top or bottom of the box.

Structural model of rat barrel cortex

NeuroNet: We reverse engineered the structural composition of the neuropil for the rat barrel cortex by using NeuroNet, a custom-designed extension package for Amira software (FEI). NeuroNet was

described in detail previously (*19*). Briefly, NeuroNet requires the following anatomical data as input **(Fig. S2)**: (i) a reconstruction of the 3D geometry and cytoarchitecture for the cortical volume of interest, (ii) a spatially dense reconstruction of the distributions of excitatory (EXC) and inhibitory (INH) neuron somata within the volume, (iii) samples of *in vivo* labeled dendrite and axon reconstructions that represent neurons from all layers and for all major morphological cell types, and (iv) cell type- and target layer-specific measurements for the densities of pre- and postsynaptic structures along these axons and dendrites, respectively. The output by NeuroNet is a digital model of the cortical volume where each neuron soma is represented by one axon and dendrite morphology from the sample of morphologies.

Anatomical input data: All anatomical data used here as input for NeuroNet was acquired in Wistar rats (primarily during the fifth postnatal week) and has been reported previously. Briefly, to capture the rat barrel cortex' characteristic geometrical, cytoarchitectonic, and cellular organization in the model, we reconstructed precise 3D maps of cortical barrel columns with surface reconstructions of the pia and white matter (*24*), and quantified the locations of all EXC and INH neuron somata in the rat barrel cortex and in VPM thalamus (*25*). To capture the rat barrel cortex' cell type-specific morphological organization in the model, we reconstructed a sample of *in vivo* labeled EXC neuron morphologies (*31, 48, 49*) and the intracortical part of *in vivo* labeled VPM axon morphologies (*50*). NeuroNet replaced each neuron of the reconstructed distribution of EXC somata with a morphology from this sample of reconstructions. The neurons' locations in the model were on average within ±119 µm of their 'true' 3D soma positions (*24*). We placed as many thalamocortical axons as the average measured number of neurons per respective VPM barreloid. Each VPM axon was displaced randomly by ±50 µm. To account for EXC connections onto INH neurons, we incorporated reconstructions of INH neurons into the model (*51-54*). *In vitro* labeled INH dendrites were 'curated' by assuming radial symmetry of their morphologies. Connections from or onto INH neurons were hence not systematically analyzed unless. To capture the rat barrel cortex' distribution of synaptic structures in the model, we derived the number of presynaptic structures (i.e., axonal boutons) by multiplying the axon length that each neuron contributes to a particular subvolume with the number of boutons per length (*19*), as measured for all EXC cell types and layer 1 INH neurons, and depending on the axons' target layer (*31, 54*). For all remaining INH neurons we set the density to 0.2 boutons per µm axon as reported in (*55-57*). Based on the resulting density distribution of boutons along the cortical depth, we scaled the total number of postsynaptic structures along the dendrites. More specifically, we performed the scaling separately for targets of boutons along EXC and INH axons: First, for targets of EXC boutons, we derived the number of postsynaptic structures along EXC dendrites (i.e., spines) by assuming that spine densities are proportional to dendritic length. For the respective number of postsynaptic structures along INH dendrites and somata we assumed proportionality to their respective surface areas. The derived density of postsynaptic structures for EXC neurons ranged from 1.04 to 1.68 spines per µm dendritic length, consistent with empirical spine density measurements (*58, 59*). The derived density of postsynaptic structures for INH neurons was 0.74 per µm² of dendritic or somatic surface, consistent with empirical synapse density measurements on INH somata (*60, 61*). Second, for targets of INH boutons, we derived the number of postsynaptic structures along both EXC and INH dendrites and somata by assuming proportionality to their respective surface areas. The derived density of postsynaptic structures for EXC and INH neurons was 0.06 per µm² of dendritic and somatic surface, consistent with empirical data (*60-62*).

Morphological variability analysis: We tested how representative the sample of EXC axon and dendrite morphologies is. For this, we performed the following analysis: First, we aligned the dendrite morphologies of each cell type by their lateral soma position and calculated dendrite innervation volumes at 50 µm resolution for an increasing sample of morphologies (i.e., 1, 2, etc. to maximum sample size-1). For each cell type and sample size, we determined all possible combinations of reconstructed morphologies. If there were more than 500 possible combinations, we used a random sample of 500

combinations. We calculated the differences between the respectively determined innervation volumes and that innervated by all morphologies for this type. Second, we determined the respective dendrite length contribution per subvolume of each combination of morphologies. For each sample size of morphologies, we calculated the CV of the dendrite length per subvolume across all possible combinations. We repeated the same analysis for axons without alignment by somata.

Model robustness analysis: We used NeuroNet to create >30,000 barrel cortex models with different anatomical data as input and quantified the variability across models of the structural composition for 512 (50 µm)³ large subvolumes within layers 2 to 6 of the C2 barrel column – i.e., axonal and dendritic path length, number of branches, number of branches that remain unconnected to a soma within the same subvolume, number of synapses (i.e., boutons), number of contributing cells and cell types, and path length to soma of each branch. First, we assessed how these parameters of the structural composition are affected by the limited sample size of morphology reconstructions. For this, we generated models where only one morphology per cell type, two morphologies, and so on were used as input to NeuroNet. Starting with one morphology per type, we used a random sample of 500 combinations of morphologies as input to generate 500 models. All models were based on the same dense distribution of neuron somata (i.e., average across measurements from four barrel cortices (*25*)). For each of the subvolumes, we determined the CV of each structural feature across the 500 models. We then calculated the median CV of each structural feature across all subvolumes. We refer to the median CV as the 'morphological uncertainty' per subvolume. We repeated this analysis for two morphologies per cell type and so on until the maximal sample size of morphologies was reached, respectively. Second, we assessed how the parameters of the structural composition are affected by the variability of soma distributions across animals. For this, we repeated the analysis of 'morphological uncertainty' with models that were based on each of the four measured dense distribution of neuron somata that were used to create an average distribution (*25*). We again calculated the median CV of each structural feature across all subvolumes and refer to the median CV as the 'cellular uncertainty' per subvolume.

Generation of statistical ensembles of connectomes

We derived the statistical ensemble of connectomes for the dense model of rat barrel cortex by assuming that only the presence of a pre- and postsynaptic structure within the same subvolume is necessary for synapse formation – i.e., their particular positions or proximity (e.g. touch) within a subvolume are not considered (*19*). First, we calculated the *dense structural overlap* ($\boldsymbol{DSO}$) as the product of the numbers of pre- and postsynaptic structures that neurons $\boldsymbol{i}$ and $\boldsymbol{j}$ contribute to a subvolume $\boldsymbol{x}$, relative to the total number of postsynaptic structures contributed by all neurons, here indexed with $\boldsymbol{N}$.

$$DSO_{(i,j,x)} = PRE_{(i,x)} \cdot \frac{POST_{(j,x)}}{\sum_N POST_{(N,x)}} \qquad \textbf{Equation (1)}$$

Based on this quantity, we assume that any presynaptic structure has equal probability of forming a connection with any of the available postsynaptic structures present within the same subvolume. The probability $\boldsymbol{p}$ for the presence of $\boldsymbol{n}$ connections between neurons $\boldsymbol{i}$ and $\boldsymbol{j}$ within a subvolume $\boldsymbol{x}$ across all possible networks is therefore given by a Poisson distribution with parameter $\boldsymbol{n}$:

$$p_{(i,j,x,n)} = \frac{DSO_{(i,j,x)}{}^{n}}{n!} \cdot e^{-DSO_{(i,j,x)}} \qquad \textbf{Equation (2)}$$

We assume that the formation of connections does not affect synapse formation elsewhere. Thus, the probability $\boldsymbol{P}$ that neurons $\boldsymbol{i}$ and $\boldsymbol{j}$ are connected by ≥1 synapse across all possible networks is given by:

$$P_{(i,j)} = 1 - e^{-\sum_k DSO_{(i,j,x_k)}} = 1 - \prod_k e^{-DSO_{(i,j,x_k)}} \qquad \textbf{Equation (3)}$$

where the index $\boldsymbol{k}$ runs over all subvolumes in which neurons $\boldsymbol{i}$ and $\boldsymbol{j}$ overlap. Parameterizing the subvolumes of the barrel cortex model by the quantity $\boldsymbol{DSO}$, followed by application of equations 2-3, thereby yielded the statistical ensemble of connectomes analyzed here. We calculated the statistical ensemble of connectomes for subvolumes of (50 µm)³ unless otherwise stated. The color map of the matrix representation in **Figure 1F** was limited to 95% of the connection probability values (i.e., to 55%).

Quantification and statistical analysis

Testing of Peters' Rule: To test Peters' Rule at the subcellular level we restricted our analysis to the structural composition of layers 2 to 6 within the C2 barrel column. Within that volume, we calculated the number of boutons and branch pairs that form zero to eight or more synapses per (50 µm)³ large subvolumes (n=512). We repeated this analysis for 512 subvolumes with 1, 5, 10, and 25 µm edge lengths and for 64 subvolumes with 100 µm edge length. At 1 µm edge length we excluded 229 subvolumes where either no axon or no dendrite were present. To test Peters' Rule at the cellular level we restricted our analysis to a combination of ~400 million neuron pairs. For each pair, we determined the number of (50 µm)³ large subvolumes with axo-dendritic overlap, referred to as $\boldsymbol{n_{overlap}}$. We then calculated in how many networks the pair forms zero to $\boldsymbol{n_{overlap}}$ synapses across all subvolumes. The resulting occurrences represent an upper bound since we constrained the overall number of connections and not the number of connections per subvolume. We mapped the number of connections per pair on bins of 1% width ranging from 0% (no connection between pair) to 100% (as many connections as $\boldsymbol{n_{overlap}}$). Finally, we determined the average number of occurrences across all pairs per bin. The resulting profile was smoothed with a moving median for visualization purposes. We determined how many of ~400 million pairs overlap at 1, 5, 10, 25 and 100 µm edge length and how often those were connected in the model.

Analyses of statistical ensemble of connectomes: We used the Matlab built-in *digraph* to illustrate two possible networks of 50 neurons as a graph. Edges between neurons were realized based on their predicted connection probability in the statistical ensemble of connectomes. We constrained each network to have the same number of edges. We generated the random network example by randomly assigning the same number of edges to 50 neurons. To analyze network topologies, we calculated the occurrence probability of each of the 15 motifs for a set of 8 million randomly selected neuron triplets with each neuron belonging to a particular neuron population (e.g. neurons were grouped by their cell type or soma position in a layer). We calculated the mean probability of the occurrences for each motif as predicted by the statistical ensemble of connectomes and compared it with those expected in a random network: First, we calculated the mean connection probabilities for each of the six edges between all of the sampled neurons. Second, we used these six mean connection probabilities to calculate the occurrence probability of each motif. Third, we divided the predicted motif probabilities by their respective expected probabilities in the random network. We calculated the deviation of motif occurrences of all 15 motifs for all 220 cell type-specific triplet combinations. For each triplet combination we calculated the mean and CV of their connection probability distribution across all six edges. For triplets with neurons from at least two different cell types (n=210), we also calculated the mean across all in-degree correlation coefficients involving these cell types. We extended our analysis to motifs between more than three neurons. We computed the probabilities of motif 1 (recurrent loop) and 13 (feedforward chain) for up to ten neurons. For this, we randomly sampled sets of neurons per motif size (10 million for each motif) from the statistical ensemble of connectomes (i.e., 3 to 10) and computed the occurrence probabilities, respectively. We compared the respective probabilities with those computed in random networks based on the mean connection probability across all neurons of the sample. We computed the mean, standard deviation, and CV, of the connection probabilities between all cell type groupings. We assessed correlations between neurons by calculating the number of incoming edges $\boldsymbol{n_{EDGES}}$ between presynaptic neurons $\boldsymbol{i}$ (including those from VPM thalamus) and postsynaptic neurons $\boldsymbol{j}$ by summing their respective $\boldsymbol{DSO}$ across all overlapping (50 µm)³ large subvolumes $\boldsymbol{x}$:

$$n_{EDGES}(i,j) = \sum_k DSO_{(i,j,x_k)} \qquad \textbf{Equation (4)}$$

We grouped all pre- and postsynaptic neurons by their cell type identity, and summed $\boldsymbol{n_{EDGES}(i,j)}$ across each presynaptic population. This resulted in the mean number of connections (i.e., in-degree) each postsynaptic neuron ***j*** receives from this population across networks. We computed a linear regression fit and Pearson's linear correlation coefficient between the in-degrees of two different presynaptic populations onto all neurons per postsynaptic cell type. We repeated this computation for all possible combinations of presynaptic cell types.

Comparison with empirical data: We calculated the occurrences that two branches form zero, one, two, three, and (at least) four synapses for all branch pairs for a sample of 252 subvolumes of 100x100x50 µm³ in layer 4 for comparison with the empirical data reported for layer 4 of mouse barrel cortex (*13*). We compared our predictions with 89 empirical connection probability measurements reported across a set of 29 studies (*11, 16, 32-35, 63-85*). We emulated the respective experimental conditions in the model. For empirical data from *in vitro* studies, we created twenty virtual brain slices of 300 µm thickness through the model **(Fig. S6)**. The slices were shifted by 20 µm with respect to one another along the rostro-caudal axis. We truncated the neurites of all neurons whose somata were located within each slice (i.e., we cut branches at their intersection with the slice surface, and removed those branches from the model that became disconnected from the soma). We computed the connection probabilities between each neuron pair in the virtual slices as defined by **Equations 1-3** with the quantity $\boldsymbol{DSO}$ being the contribution of pre- and postsynaptic structures by the truncated pairs' morphologies with respect to the total number of postsynaptic structures contributed by all neurons. We grouped the neurons as described in the respective studies (**Table S1**); i.e., by their laminar soma location and – if reported – by their cell type. Layer borders were defined as reported previously (*25*). If the recording depth underneath the slice surface was not reported, we restricted the comparison to pairs within the mean reported range of recording depths (31 µm to 130 µm). We computed the Pearson's linear correlation coefficient between the empirical and predicted connection probabilities and the 95% confidence bounds for new observations based on a linear regression with no intercept using the Matlab built-ins *fitlm* and *predict*. We performed a random permutation test on the correlation coefficient by shuffling the empirical and the predicted connection probabilities and re-computing their correlation coefficient. We repeated this step 100,000 times. We compared the model predictions with two empirical studies that performed connectivity measurements as a function of inter-somatic distance (*32, 63*) (**Tables S2-3**). Here, we grouped neurons additionally by their inter-somatic distance along the lateral axis (i.e., the axis running parallel to the slicing surface). We compared the predicted deviations of motif occurrences across L5PT triplets and doublets with empirical observations (*16*). We grouped the neurons accordingly and calculated the motif occurrences and ratios for ~1.7 million L5PT doublets and ~200,000 L5PT triplets across 20 slice models. We used the same analysis as reported by (*16*) and normalized the resulting triplet ratios by the doublet motif occurrences to avoid over- or underrepresentation of triplet motifs due to over- or underrepresentation of doublet motifs. We compared the motif probabilities across the number of edges in motifs of eight neurons in the barrel cortex model and a random network to empirical observations (*32*). For this, we randomly sampled 20,000 sets of eight L5PTs across 20 slice models. For each set of neurons and each number of possible edges (ranging from 0 to 56 possible edges), we computed the number of possible edge combinations (e.g., 1 possible combination of 0 or 56 edges, but more than 10^{10} possible combinations of 10 edges). If the number of edge combinations was less than 1,000, we iterated over all possible combinations. If the number of combinations was larger than 1,000, we randomly generated 1,000 motifs that matched the number of edges. We calculated the respective (occurrence) probability of each edge motif in the slice models and a random network constrained by the respective mean connection probability.

References

1. S. H. Bennett, A. J. Kirby, G. T. Finnerty, Rewiring the connectome: Evidence and effects. *Neurosci Biobehav Rev* **88**, 51-62 (2018).
2. K. P. Berry, E. Nedivi, Spine Dynamics: Are They All the Same? *Neuron* **96**, 43-55 (2017).
3. J. L. Lefebvre, J. R. Sanes, J. N. Kay, Development of dendritic form and function. *Annu Rev Cell Dev Biol* **31**, 741-777 (2015).
4. J. R. Sanes, M. Yamagata, Many paths to synaptic specificity. *Annu Rev Cell Dev Biol* **25**, 161-195 (2009).
5. S. Yogev, K. Shen, Cellular and molecular mechanisms of synaptic specificity. *Annu Rev Cell Dev Biol* **30**, 417-437 (2014).
6. C. L. Rees, K. Moradi, G. A. Ascoli, Weighing the Evidence in Peters' Rule: Does Neuronal Morphology Predict Connectivity? *Trends Neurosci* **40**, 63-71 (2017).
7. V. Braitenberg, A. Schüz, in *Anatomy of the cortex*. (Springer, 1991), pp. 109-112.
8. A. Peters, M. L. Feldman, The projection of the lateral geniculate nucleus to area 17 of the rat cerebral cortex. I. General description. *J Neurocytol* **5**, 63-84 (1976).
9. Y. Mishchenko *et al.*, Ultrastructural analysis of hippocampal neuropil from the connectomics perspective. *Neuron* **67**, 1009-1020 (2010).
10. K. L. Briggman, M. Helmstaedter, W. Denk, Wiring specificity in the direction-selectivity circuit of the retina. *Nature* **471**, 183-188 (2011).
11. S. P. Brown, S. Hestrin, Intracortical circuits of pyramidal neurons reflect their long-range axonal targets. *Nature* **457**, 1133-1136 (2009).
12. N. Kasthuri *et al.*, Saturated Reconstruction of a Volume of Neocortex. *Cell* **162**, 648-661 (2015).
13. A. Motta *et al.*, Dense connectomic reconstruction in layer 4 of the somatosensory cortex. *Science* **366**, (2019).
14. S. Holler, G. Kostinger, K. A. C. Martin, G. F. P. Schuhknecht, K. J. Stratford, Structure and function of a neocortical synapse. *Nature* **591**, 111-116 (2021).
15. R. Milo *et al.*, Network motifs: simple building blocks of complex networks. *Science* **298**, 824-827 (2002).
16. S. Song, P. J. Sjostrom, M. Reigl, S. Nelson, D. B. Chklovskii, Highly nonrandom features of synaptic connectivity in local cortical circuits. *Plos Biol* **3**, e68 (2005).
17. D. Miner, J. Triesch, Plasticity-Driven Self-Organization under Topological Constraints Accounts for Non-random Features of Cortical Synaptic Wiring. *PLoS Comput Biol* **12**, e1004759 (2016).
18. T. Binzegger, R. J. Douglas, K. A. Martin, A quantitative map of the circuit of cat primary visual cortex. *J Neurosci* **24**, 8441-8453 (2004).
19. R. Egger, V. J. Dercksen, D. Udvary, H. C. Hege, M. Oberlaender, Generation of dense statistical connectomes from sparse morphological data. *Front Neuroanat* **8**, 129 (2014).
20. E. Gal *et al.*, Rich cell-type-specific network topology in neocortical microcircuitry. *Nat Neurosci* **20**, 1004-1013 (2017).
21. E. Gal, R. Perin, H. Markram, M. London, I. Segev. (www.biorxiv.org, 2019).
22. J. W. Gibbs, *Elementary Principles in Statistical Mechanics*. (New York: Charles Scribner's Sons, 1902).
23. R. T. Narayanan, D. Udvary, M. Oberlaender, Cell Type-Specific Structural Organization of the Six Layers in Rat Barrel Cortex. *Front Neuroanat* **11**, 91 (2017).
24. R. Egger, R. T. Narayanan, M. Helmstaedter, C. P. de Kock, M. Oberlaender, 3D reconstruction and standardization of the rat vibrissal cortex for precise registration of single neuron morphology. *PLoS Comput Biol* **8**, e1002837 (2012).
25. H. S. Meyer *et al.*, Cellular organization of cortical barrel columns is whisker-specific. *Proc Natl Acad Sci U S A* **110**, 19113-19118 (2013).
26. V. Braitenberg, A. Schüz, *Cortex: statistics and geometry of neuronal connectivity.*, (Springer, 1998).
27. M. Helmstaedter, Cellular-resolution connectomics: challenges of dense neural circuit reconstruction. *Nat Methods* **10**, 501-507 (2013).

28. A. Santuy, J. R. Rodriguez, J. DeFelipe, A. Merchan-Perez, Volume electron microscopy of the distribution of synapses in the neuropil of the juvenile rat somatosensory cortex. *Brain Struct Funct* **223**, 77-90 (2018).
29. S. Chandrasekaran *et al.*, Unbiased, High-Throughput Electron Microscopy Analysis of Experience-Dependent Synaptic Changes in the Neocortex. *J Neurosci* **35**, 16450-16462 (2015).
30. J. H. Macke, M. Opper, M. Bethge, Common input explains higher-order correlations and entropy in a simple model of neural population activity. *Phys Rev Lett* **106**, 208102 (2011).
31. R. T. Narayanan *et al.*, Beyond Columnar Organization: Cell Type- and Target Layer-Specific Principles of Horizontal Axon Projection Patterns in Rat Vibrissal Cortex. *Cereb Cortex* **25**, 4450-4468 (2015).
32. R. Perin, T. K. Berger, H. Markram, A synaptic organizing principle for cortical neuronal groups. *Proc Natl Acad Sci U S A* **108**, 5419-5424 (2011).
33. R. M. Bruno, B. Sakmann, Cortex is driven by weak but synchronously active thalamocortical synapses. *Science* **312**, 1622-1627 (2006).
34. Q. Q. Sun, J. R. Huguenard, D. A. Prince, Barrel cortex microcircuits: thalamocortical feedforward inhibition in spiny stellate cells is mediated by a small number of fast-spiking interneurons. *Journal of Neuroscience* **26**, 1219-1230 (2006).
35. Y. Yoshimura, J. L. Dantzker, E. M. Callaway, Excitatory cortical neurons form fine-scale functional networks. *Nature* **433**, 868-873 (2005).
36. Y. Kubota, Untangling GABAergic wiring in the cortical microcircuit. *Curr Opin Neurobiol* **26**, 7-14 (2014).
37. G. Quattrocolo, G. Fishell, T. J. Petros, Heterotopic Transplantations Reveal Environmental Influences on Interneuron Diversity and Maturation. *Cell Rep* **21**, 721-731 (2017).
38. Y. Ishino *et al.*, Regional Cellular Environment Shapes Phenotypic Variations of Hippocampal and Neocortical Chandelier Cells. *J Neurosci* **37**, 9901-9916 (2017).
39. M. A. Lanuza *et al.*, Axonal competition and synapse elimination during neuromuscular junction development. *Current Opinion in Physiology* **4**, 25-31 (2018).
40. S. G. Turney, J. W. Lichtman, Reversing the outcome of synapse elimination at developing neuromuscular junctions in vivo: evidence for synaptic competition and its mechanism. *Plos Biol* **10**, e1001352 (2012).
41. A. A. Penn, P. A. Riquelme, M. B. Feller, C. J. Shatz, Competition in retinogeniculate patterning driven by spontaneous activity. *Science* **279**, 2108-2112 (1998).
42. S. J. Cook *et al.*, The connectome of the Caenorhabditis elegans pharynx. *J Comp Neurol* **528**, 2767-2784 (2020).
43. I. D. Landau, R. Egger, V. J. Dercksen, M. Oberlaender, H. Sompolinsky, The Impact of Structural Heterogeneity on Excitation-Inhibition Balance in Cortical Networks. *Neuron* **92**, 1106-1121 (2016).
44. A. M. Zador, A critique of pure learning and what artificial neural networks can learn from animal brains. *Nat Commun* **10**, 3770 (2019).
45. B. G. Rash, E. A. Grove, Area and layer patterning in the developing cerebral cortex. *Curr Opin Neurobiol* **16**, 25-34 (2006).
46. D. E. Feldman, M. Brecht, Map plasticity in somatosensory cortex. *Science* **310**, 810-815 (2005).
47. K. C. Catania, Behavioral pieces of neuroethological puzzles. *J Comp Physiol A Neuroethol Sens Neural Behav Physiol* **203**, 677-689 (2017).
48. C. P. de Kock, R. M. Bruno, H. Spors, B. Sakmann, Layer- and cell-type-specific suprathreshold stimulus representation in rat primary somatosensory cortex. *J Physiol* **581**, 139-154 (2007).
49. M. Oberlaender *et al.*, Cell type-specific three-dimensional structure of thalamocortical circuits in a column of rat vibrissal cortex. *Cereb Cortex* **22**, 2375-2391 (2012).
50. M. Oberlaender, A. Ramirez, R. M. Bruno, Sensory experience restructures thalamocortical axons during adulthood. *Neuron* **74**, 648-655 (2012).

51. M. Arzt, B. Sakmann, H. S. Meyer, Anatomical Correlates of Local, Translaminar, and Transcolumnar Inhibition by Layer 6 GABAergic Interneurons in Somatosensory Cortex. *Cereb Cortex* **28**, 2763-2774 (2018).
52. M. Helmstaedter, B. Sakmann, D. Feldmeyer, L2/3 interneuron groups defined by multiparameter analysis of axonal projection, dendritic geometry, and electrical excitability. *Cereb Cortex* **19**, 951-962 (2009).
53. C. Koelbl, M. Helmstaedter, J. Lubke, D. Feldmeyer, A barrel-related interneuron in layer 4 of rat somatosensory cortex with a high intrabarrel connectivity. *Cereb Cortex* **25**, 713-725 (2015).
54. R. Egger *et al.*, Robustness of sensory-evoked excitation is increased by inhibitory inputs to distal apical tuft dendrites. *Proc Natl Acad Sci U S A* **112**, 14072-14077 (2015).
55. F. Karube, Y. Kubota, Y. Kawaguchi, Axon branching and synaptic bouton phenotypes in GABAergic nonpyramidal cell subtypes. *J Neurosci* **24**, 2853-2865 (2004).
56. H. Markram *et al.*, Interneurons of the neocortical inhibitory system. *Nat Rev Neurosci* **5**, 793-807 (2004).
57. Y. Wang, A. Gupta, M. Toledo-Rodriguez, C. Z. Wu, H. Markram, Anatomical, physiological, molecular and circuit properties of nest basket cells in the developing somatosensory cortex. *Cereb Cortex* **12**, 395-410 (2002).
58. A. U. Larkman, Dendritic morphology of pyramidal neurones of the visual cortex of the rat: III. Spine distributions. *J Comp Neurol* **306**, 332-343 (1991).
59. Y. Kawaguchi, F. Karube, Y. Kubota, Dendritic branch typing and spine expression patterns in cortical nonpyramidal cells. *Cereb Cortex* **16**, 696-711 (2006).
60. A. Keller, E. L. White, Synaptic organization of GABAergic neurons in the mouse SmI cortex. *J Comp Neurol* **262**, 1-12 (1987).
61. B. Ahmed, J. C. Anderson, K. A. Martin, J. C. Nelson, Map of the synapses onto layer 4 basket cells of the primary visual cortex of the cat. *J Comp Neurol* **380**, 230-242 (1997).
62. E. L. White, G. Benshalom, S. M. Hersch, Thalamocortical and other synapses involving nonspiny multipolar cells of mouse SmI cortex. *J Comp Neurol* **229**, 311-320 (1984).
63. M. Avermann, C. Tomm, C. Mateo, W. Gerstner, C. C. Petersen, Microcircuits of excitatory and inhibitory neurons in layer 2/3 of mouse barrel cortex. *J Neurophysiol* **107**, 3116-3134 (2012).
64. A. P. Bannister, A. M. Thomson, Dynamic properties of excitatory synaptic connections involving layer 4 pyramidal cells in adult rat and cat neocortex. *Cereb Cortex* **17**, 2190-2203 (2007).
65. M. Beierlein, B. W. Connors, Short-term dynamics of thalamocortical and intracortical synapses onto layer 6 neurons in neocortex. *J Neurophysiol* **88**, 1924-1932 (2002).
66. M. Beierlein, J. R. Gibson, B. W. Connors, Two dynamically distinct inhibitory networks in layer 4 of the neocortex. *J Neurophysiol* **90**, 2987-3000 (2003).
67. R. M. Bruno, D. J. Simons, Feedforward mechanisms of excitatory and inhibitory cortical receptive fields. *J Neurosci* **22**, 10966-10975 (2002).
68. C. M. Constantinople, R. M. Bruno, Deep cortical layers are activated directly by thalamus. *Science* **340**, 1591-1594 (2013).
69. S. R. Crandall, S. L. Patrick, S. J. Cruikshank, B. W. Connors, Infrabarrels Are Layer 6 Circuit Modules in the Barrel Cortex that Link Long-Range Inputs and Outputs. *Cell Rep* **21**, 3065-3078 (2017).
70. D. Feldmeyer, V. Egger, J. Lubke, B. Sakmann, Reliable synaptic connections between pairs of excitatory layer 4 neurones within a single 'barrel' of developing rat somatosensory cortex. *J Physiol* **521 Pt 1**, 169-190 (1999).
71. D. Feldmeyer, J. Lubke, B. Sakmann, Efficacy and connectivity of intracolumnar pairs of layer 2/3 pyramidal cells in the barrel cortex of juvenile rats. *J Physiol* **575**, 583-602 (2006).
72. D. Feldmeyer, J. Lubke, R. A. Silver, B. Sakmann, Synaptic connections between layer 4 spiny neurone-layer 2/3 pyramidal cell pairs in juvenile rat barrel cortex: physiology and anatomy of interlaminar signalling within a cortical column. *J Physiol-London* **538**, 803-822 (2002).

73. D. Feldmeyer, A. Roth, B. Sakmann, Monosynaptic connections between pairs of spiny stellate cells in layer 4 and pyramidal cells in layer 5A indicate that lemniscal and paralemniscal afferent pathways converge in the infragranular somatosensory cortex. *J Neurosci* **25**, 3423-3431 (2005).
74. S. B. Hofer *et al.*, Differential connectivity and response dynamics of excitatory and inhibitory neurons in visual cortex. *Nat Neurosci* **14**, 1045-1052 (2011).
75. C. Holmgren, T. Harkany, B. Svennenfors, Y. Zilberter, Pyramidal cell communication within local networks in layer 2/3 of rat neocortex. *J Physiol* **551**, 139-153 (2003).
76. X. Jiang *et al.*, Principles of connectivity among morphologically defined cell types in adult neocortex. *Science* **350**, aac9462 (2015).
77. J. S. Jouhanneau, J. Kremkow, A. L. Dorrn, J. F. Poulet, In Vivo Monosynaptic Excitatory Transmission between Layer 2 Cortical Pyramidal Neurons. *Cell Rep* **13**, 2098-2106 (2015).
78. J. S. Jouhanneau, J. Kremkow, J. F. A. Poulet, Single synaptic inputs drive high-precision action potentials in parvalbumin expressing GABA-ergic cortical neurons in vivo. *Nat Commun* **9**, 1540 (2018).
79. P. Krieger, T. Kuner, B. Sakmann, Synaptic connections between layer 5B pyramidal neurons in mouse somatosensory cortex are independent of apical dendrite bundling. *J Neurosci* **27**, 11473-11482 (2007).
80. S. Lefort, C. Tomm, J. C. Floyd Sarria, C. C. Petersen, The excitatory neuronal network of the C2 barrel column in mouse primary somatosensory cortex. *Neuron* **61**, 301-316 (2009).
81. H. Markram, J. Lubke, M. Frotscher, A. Roth, B. Sakmann, Physiology and anatomy of synaptic connections between thick tufted pyramidal neurones in the developing rat neocortex. *J Physiol* **500 (Pt 2)**, 409-440 (1997).
82. A. Mercer *et al.*, Excitatory connections made by presynaptic cortico-cortical pyramidal cells in layer 6 of the neocortex. *Cereb Cortex* **15**, 1485-1496 (2005).
83. C. C. Petersen, B. Sakmann, The excitatory neuronal network of rat layer 4 barrel cortex. *J Neurosci* **20**, 7579-7586 (2000).
84. G. Silberberg, H. Markram, Disynaptic inhibition between neocortical pyramidal cells mediated by Martinotti cells. *Neuron* **53**, 735-746 (2007).
85. A. M. Thomson, D. C. West, Y. Wang, A. P. Bannister, Synaptic connections and small circuits involving excitatory and inhibitory neurons in layers 2-5 of adult rat and cat neocortex: triple intracellular recordings and biocytin labelling in vitro. *Cereb Cortex* **12**, 936-953 (2002).

Acknowledgments

We thank Kevin Briggman and Peter L. Strick for discussions and advice; Vincent J. Dercksen and Robert Egger for developing early versions of the model; and Haim Sompolinsky and Idan Segev for comments on the manuscript. Funding was provided from the Center of Advanced European Studies and Research, the Max Planck Institute for Biological Cybernetics, the Center for Neurogenomics and Cognitive Research, the European Research Council under the European Union's Horizon 2020 research and innovation program (grant agreement 633428; to M.O.), the German Federal Ministry of Education and Research (grants BMBF/FKZ 01GQ1002 and 01IS18052; to M.O. and J.M.), and the Deutsche Forschungsgemeinschaft (SFB 1089 and SPP 2041 to M.O. and J.M.; and EXC number 2064/1, 39072764 to J.M.); **Author contributions:** M.O. conceived and designed the study. D.U. developed the model and analysis routines. P.H. and H.H. developed the online model. J.M. developed the mathematical model. C.K. and B.S. provided data. D.U., P.H. and M.O. analyzed the data, and M.O. wrote the paper with help from all authors. **Declaration of Interests:** The authors declare no competing interests.